AJNR

Visualization of the Extracranial Branches of the Trigeminal Nerve Using Improved Motion-Sensitized Driven Equilibrium–Prepared 3D Inversion Recovery TSE Sequence

Dejun She, Hao Huang, Dongmei Jiang, Junhuan Hong, Peiying You, Lu Li, Xiance Zhao and Dairong Cao

AJNR Am J Neuroradiol published online 4 July 2024
http://www.ajnr.org/content/early/2024/07/04/ajnr.A8273

Published July 4, 2024 as 10.3174/ajnr.A8273

Visualization of the Extracranial Branches of the Trigeminal Nerve Using Improved Motion-Sensitized Driven Equilibrium–Prepared 3D Inversion Recovery TSE Sequence

Dejun She, Hao Huang, Dongmei Jiang, Junhuan Hong, Peiying You, Lu Li, Xiance Zhao, and Dairong Cao

ABSTRACT

BACKGROUND AND PURPOSE: Visualization of the extracranial trigeminal nerve is crucial to detect nerve pathologic alterations. This study aimed to evaluate visualization of the extracranial trigeminal nerve using 3D inversion recovery TSE with an improved motion-sensitized driven equilibrium (iMSDE) pulse.

MATERIALS AND METHODS: In this prospective study, 35 subjects underwent imaging of the trigeminal nerve using conventional 3D inversion recovery TSE, 3D inversion recovery TSE with an iMSDE pulse, and contrast-enhanced 3D inversion recovery TSE. The visibility of 7 extracranial branches of the trigeminal nerve, venous/muscle suppression, and identification of the relationship between nerves and lesions were scored on a 5-point scale system. In addition, SNR, nerve-muscle contrast ratio, nerve-venous contrast ratio, nerve-muscle contrast-to-noise ratio, and nerve-venous contrast-to-noise ratio were calculated and compared.

RESULTS: Images acquired with iMSDE 3D inversion recovery TSE had significantly higher nerve-muscle contrast ratio, nerve-venous contrast ratio, and nerve-to-venous contrast-to-noise ratio (all $P < .001$); improved venous/muscle suppression and clearer visualization of the trigeminal nerve branches except the ophthalmic nerve than with conventional 3D inversion recovery TSE (all $P < .05$). Compared with contrast-enhanced 3D inversion recovery TSE, images acquired with iMSDE 3D inversion recovery TSE had significantly higher SNR, nerve-muscle contrast ratio, and nerve-to-venous contrast-to-noise ratio (all $P < .05$), and demonstrated comparable diagnostic quality (scores ≥ 3) of the maxillary nerve, mandibular nerve, inferior alveolar nerve, lingual nerve, and masseteric nerve ($P > .05$). As for the identification of the relationship between nerves and lesions, iMSDE 3D inversion recovery TSE showed the highest scores among these 3 sequences (all $P < .05$).

CONCLUSIONS: The iMSDE 3D inversion recovery TSE is a promising alternative to conventional 3D inversion recovery TSE and contrast-enhanced 3D inversion recovery TSE for visualization of the extracranial branches of trigeminal nerve in clinical practice.

ABBREVIATIONS: CNR_{nm} = nerve-to-muscle contrast-to-noise ratio; CNR_{nv} = nerve-to-venous contrast-to-noise ratio; CR_{nm} = nerve-to-muscle contrast ratio; CR_{nv} = nerve-to-venous contrast ratio; ICC = intraclass correlation coefficient; IR-TSE = inversion recovery turbo spin echo; iMSDE = improved motion-sensitized driven equilibrium; MRN = MR neurography

The trigeminal nerve is the largest cranial nerve and is extensively distributed in the head and neck.[1] The extracranial branches of the trigeminal nerve are numerous and can be involved in myriad disease entities, including tumors, inflammations, traumatic or iatrogenic injuries, radiation treatment, and degenerative disorders.[2-4] Visualization of the extracranial trigeminal nerve is crucial for detecting pathologic alterations and differentiating pathologic causes of trigeminal nerve–involved diseases.[5-8] Due to the advent of high-field MRI devices and improved imaging techniques, MR neurography (MRN), which selectively enhances the visualization of nerves, has become a potentially promising and integrating strategy in diagnosing neuropathies.[1,9] However, many factors, including surrounding tissue signals and motion artifacts on MRN, may affect the visualization of the extracranial trigeminal nerve and hamper the correct diagnosis. Consequently, there are still huge challenges in delineating the entire course of the extracranial trigeminal nerve using MRN.

Received January 31, 2023; accepted after revision February 28, 2024.

From the Department of Radiology (D.S., H.H., D.J., J.H., P.Y., D.C.) and Key Laboratory of Radiation Biology of Fujian Higher Education Institutions (D.S., D.C.), First Affiliated Hospital of Fujian Medical University, Fuzhou, China; Department of Radiology (D.S., H.H., D.J., J.H., P.Y., D.C), National Regional Medical Center, Binhai Campus of the First Affiliated Hospital, School of Medical Imaging (L.L.), and Department of Radiology (D.C.), Fujian Key Laboratory of Precision Medicine for Cancer, First Affiliated Hospital, Fujian Medical University, Fuzhou, Fujian, China; and Philips Healthcare (X.Z.), Shanghai, China.

Dejun She and Hao Huang are co-first authors and contributed equally to this study.

This work was funded by the Innovation and Entrepreneurship Training Program for Undergraduates of Fujian Medical University (No. S202110392022).

Please address correspondence to Dairong Cao, MD, Department of Radiology, First Affiliated Hospital of Fujian Medical University, 20 Cha-Zhong Rd, Fuzhou, Fujian 350005, China; e-mail: dairongcao@163.com

Indicates article with online supplemental data.

http://dx.doi.org/10.3174/ajnr.A8273

Parameters of MR imaging

Parameter	Conventional 3D IR-TSE	iMSDE 3D IR-TSE	CE 3D IR-TSE
TR/TE (ms)	2800/181	2800/181	2800/181
Flip angle (degrees)	Variable flip angle	Variable flip angle	Variable flip angle
Field of view (mm)	200 × 200	200 × 200	200 × 200
Voxel size (mm)	0.9 × 0.9 × 0.9	0.9 × 0.9 × 0.9	0.9 × 0.9 × 0.9
No. of slices	210	210	210
Averages	2	2	2
Fat-suppression	STIR	STIR	STIR
iMSDE TEprep (ms)		60	/
iMSDE VENC (cm/s)		0.35	
Acquisition time (min/sec)	8 min 27 sec	8 min 27 sec	8 min 27 sec

Note:—TEprep indicates magnetization preparation TE; VENC, velocity-encoded; CE, contrast-enhanced.

Several dedicated MRI techniques have been used in the evaluation of peripheral nerves in the head and neck, such as double-echo steady-state[10,11] and reversed fast imaging in steady-state free precession.[12,13] However, as gradient-recalled echo sequences, these sequences are sensitive to magnetic field inhomogeneities, resulting in insufficient fat suppression in the neck. Thus, spin-echo-based pulse sequences are more suitable for high-resolution MRN in the neck due to homogeneous fat suppression and less sensitivity to magnetic field inhomogeneities. 3D inversion recovery TSE (3D IR-TSE) T2-weighted imaging is one of the most common sequences that can provide isotropic spatial resolution, high soft-tissue contrast, and excellent fat suppression. To date, Viallon et al[14] reported that 3D IR-TSE can accomplish the delineation and evaluation of peripheral nerve structures. Heavily T2-weighted 3D IR-TSE sequences highlight nerve structures by visualizing hyperintense signals of water and small molecule proteins in the endoneurium.[15] However, the veins and muscles are very close to the nerves, still being the main challenge of MRN in the head and neck. Specifically, the hyperintensity of the surrounding tissue such as veins and muscles can obscure the visualization of nerves on conventional 3D IR-TSE, impairing diagnostic accuracy. It has been reported that gadolinium-based contrast agents can suppress background tissue to improve the visualization of nerves.[15-17] However, the potential of nephrogenic systemic fibrosis and gadolinium deposition induced by Gd-DTPA administration limits their use in pregnant patients, children, and patients with renal insufficiency.[18]

Recently, several prior studies have focused on using a 3D IR-TSE sequence preceded by an improved motion-sensitized driven equilibrium (iMSDE) pulse to image the peripheral nerves.[19] The iMSDE technique is based on the T2 magnetization preparatory pulse and diffuse motion sensitivity in 3 directions, which could effectively suppress tissue signals with short transverse relaxation times and moving object signals (eg, blood), respectively.[19,21,22] As a novel and safe technique in MRN, the iMSDE pulse can provide uniform suppression of vessels without additional contrast agents and has been demonstrated to improve the visualization of peripheral nerves in several anatomic regions.[20–22] However, there are limited studies reporting using the iMSDE 3D IR-TSE sequence to delineate the extracranial branches of the trigeminal nerve.[23] Thus, this study aimed to evaluate the value of 3D IR-TSE with an iMSDE pulse in visualizing the extracranial branches of the trigeminal nerve by systematic comparison with conventional 3D IR-TSE and contrast-enhanced 3D IR-TSE.

MATERIALS AND METHODS

Study Design and Study Population

This prospective study was approved by the institutional review board and conducted under the Committee for Human Research of the First Affiliated Hospital of Fujian Medical University. Written informed consent was obtained from all participants. For this study, we consecutively included subjects with MRI for suspected lesions in the head and neck area. Exclusion criteria were as follows: 1) ferromagnetic implants in the head and neck, 2) contraindications to a contrast-enhanced MRI examination, 3) obvious motion-induced image artifacts, and 4) failure in scanning all sequences required.

Thirty-nine patients referred mainly by the department of otorhinolaryngology as well as oral and maxillofacial surgery were included in this study from January to September 2022. All 39 patients underwent a contrast-enhanced MR examination of the head and neck area. Four patients whose images had obvious motion artifacts were excluded. Eventually, a total of 35 subjects (20 women, 15 men; mean age, 41 years; range, 24–66 years) were included. Among them, 20 subjects who were finally confirmed to have no lesions in the head and neck area were classified as healthy controls and evaluated for the visualization of normal nerves. The other 15 patients who were confirmed to have lesions in the head and neck were enrolled and regarded as a case group.

MRI Protocol

All acquisitions were performed on a 3T whole-body MRI scanner (Ingenia; Philips Healthcare) using a 32-channel head coil. The MR imaging sequences included conventional 3D IR-TSE without an iMSDE pulse, 3D IR-TSE with an iMSDE pulse, and contrast-enhanced 3D IR-TSE without an iMSDE pulse. All sequences were scanned with the patient in the coronal position to encompass as many branches of the trigeminal nerve as possible. The detailed scan parameters of these 3 sequences are summarized in the Table. Contrast-enhanced 3D IR-TSE was performed after administration of 0.15 mmol/kg of gadobenate dimeglumine (Multihance; Bracco Diagnostics).

Image Evaluation

First, all subjects and scan information were pseudonymized, and MR images in each sequence were evaluated independently by both reviewers in random order. The original coronal images and reconstructed MIP and MPR images were combined for a more comprehensive evaluation. A total of 7 branches of the trigeminal

nerve were evaluated in this study, including the 3 divisions of trigeminal nerve (ophthalmic, maxillary, mandibular) as well as the 4 extracranial branches of the mandibular division (inferior alveolar nerve, lingual nerve, masseteric nerve, and buccal nerve), which are frequently invaded by lesions. A 5-point subjective scoring system was used to assess the visualization ability of these 3 sequences for normal nerves and the relationship between nerves and lesions. Before we performed the evaluation, a calibration session was conducted to clarify the scoring criteria according to previous scoring. When scores evaluated by the 2 observers did not agree, the decision was reached by consensus between the 2 observers. In addition, the SNR, contrast ratio (CR), and contrast-to-noise ratio (CNR) of the normal nerves were calculated.

Visualization Ability of Normal Nerve

A 5-point subjective scoring system was used to assess MRN images by 2 observers (3 and 9 years of specific MR imaging experience).

The visualization of nerves was evaluated with a modified 5-score scale[24] as follows: excellent (5), sharp nerve edges and uniform hyperintensity; good (4), sharp nerve edges and heterogeneous hyperintensity; fair (3), blurred nerve edges and moderate signal intensity poor (2), blurred or distorted nerve edges and weak signal intensity; and none (1), none of the nerves were identified (Online Supplemental Data). For diagnostic quality of the MRN images for each nerve, a nerve visualization score of ≥ 3 was considered acceptable diagnostic quality, indicating that the images met the clinical diagnostic requirements. On the contrary, a visualization score of 1–2 was considered an unacceptable diagnostic quality.

Muscle suppression and venous suppression were also evaluated with a modified 5-score scale as follows:[12] excellent (5), perfect background tissue suppression with uniform hypointensity in background tissue; good (4), good background tissue suppression with heterogeneous hypointensity in background tissue; fair (3), fair background tissue suppression with moderate signal intensity in background tissue; poor (2), poor background tissue suppression with hyperintensity in background tissue; and none (1), no background suppression.

SNR, CR, and CNR Calculation of the Normal Nerve

Another 2 radiologists (5 and 10 years of experience in MR imaging) independently measured the nerve SNR, nerve-to-muscle contrast ratio (CR_{nm}), nerve-to-venous contrast ratio (CR_{nv}), nerve-to-muscle contrast-to-noise ratio (CNR_{nm}), and nerve-to-venous CNR (CNR_{nv}) at IntelliSpace Portal (ISP, Philips Healthcare). Three successive coronal MRN images at the level of the inferior alveolar nerve and its adjacent tissue (internal pterygoid muscle and pterygoid plexus) were selected, and ROIs (1 mm^2) were manually placed. The average signal intensity (SI) of 3 ROIs was acquired. The SNR, CR_{nm}, CR_{nv}, CNR_{nm}, and CNR_{nv} were calculated by using the following equations:

$$CR = (SI_{nerve} - SI_a)/(SI_{nerve} + SI_a)$$

$$CNR = (SI_{nerve} - SI_a)/(SD_{nerve}).$$

The letter a in the formulas above represented adjacent tissues of the inferior alveolar nerve, including the internal pterygoid muscle and pterygoid plexus.

Identification Ability of the Relationship between Nerves and Lesions

The identification ability of the relationship between the peripheral branches of the trigeminal nerve and lesions was evaluated independently by 2 radiologists (3 and 9 years of specific MR imaging experience). The assessment is based on a modified 5-score scale[24] as follows: excellent (5), defined as a clear relationship between nerves and lesions; good (4), the relationship between nerves and lesions can be distinguished; fair (3), the relationship between nerves and lesions can be partially distinguished; poor (2), the relationship between nerves and lesions was blurred and difficult to determine; and none (1), none of the nerves or lesions were identified, unable to assess the relationship among them.

Statistical Analysis

All data were presented as mean (SD), median (interquartile range), or number of cases and ratio, as appropriate. Multiple tests were assessed by 1-way ANOVA with a Tukey post hoc test if data satisfied the normal distribution and homogeneous variance. On the contrary, Friedman rank-sum tests would be used if data did not satisfy the normal distribution and homogeneous variance. Post hoc tests were performed using the 2-stage linear step-up procedure proposed by Benjamini et al.[25] For 2-category data (the proportion of MRN images with acceptable diagnostic quality), the Cochran Q test was used, and the Dunn test with a Bonferroni corrections was used for pair-wise comparisons. The intraclass correlation coefficient (ICC) was used to assess interobserver agreement. A single-measurement, absolute-agreement, 2-way random effects model was used to calculate the ICCs with 95% CIs. The ICC was defined as follows: poor, <0.2; fair, 0.2–0.4; moderate, 0.4–0.6; good, 0.6–0.8; and excellent, 0.8–1.0.

Statistical analyses were performed using SPSS (Version 26.0; IBM), and graphs were created using GraphPad Prism 9 (GraphPad Software). P values $< .05$ were considered statistically significant.

RESULTS

We performed normality and homogeneity tests of variance before statistical analysis of the data. None of the data satisfied the normal distribution and homogeneous variance. Therefore, Friedman analysis was used for all quantitative data in this study.

Comparisons of Normal Nerve Visualization

According to MR imaging, 40 nerves (20 healthy subjects, each left and right side) of each branch were included for assessment of nerve visualization among the 3 sequences.

The scores of nerve visualization and muscle and venous suppression are presented in the Online Supplemental Data. As shown in the Online Supplemental Data, the iMSDE 3D IR-TSE had higher scores in visualizing the maxillary nerve, mandibular nerve, inferior alveolar nerve, lingual nerve, masseteric nerve, and buccal nerve compared with conventional 3D IR-TSE (all $P \leq .05$), except the ophthalmic nerve ($P = .26$) (Figs 1 and 2, Online Supplemental Data). The iMSDE 3D IR-TSE demonstrated the highest scores of muscle suppression followed by contrast-enhanced 3D IR-TSE (all $P < .05$). The contrast-enhanced

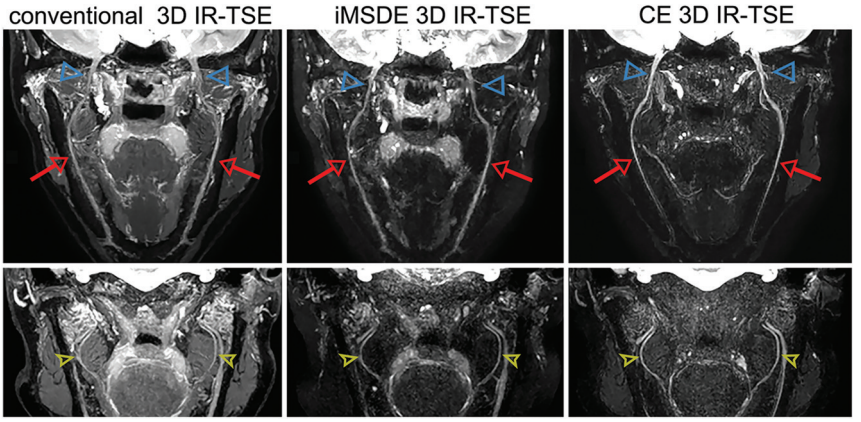

FIG 1. A 32-year-old patient with no lesion in the head and neck. Curved planar reformation MIP (2-mm layer thickness) of the mandibular nerve (*blue triangle*), inferior alveolar nerve (*red thin arrow*), and lingual nerve (*yellow arrowhead*) at the oblique coronary position. Both iMSDE 3D IR-TSE and CE 3D IR-TSE significantly improved visualization in assessing the inferior alveolar nerve and lingual nerve. CE indicates contrast-enhanced.

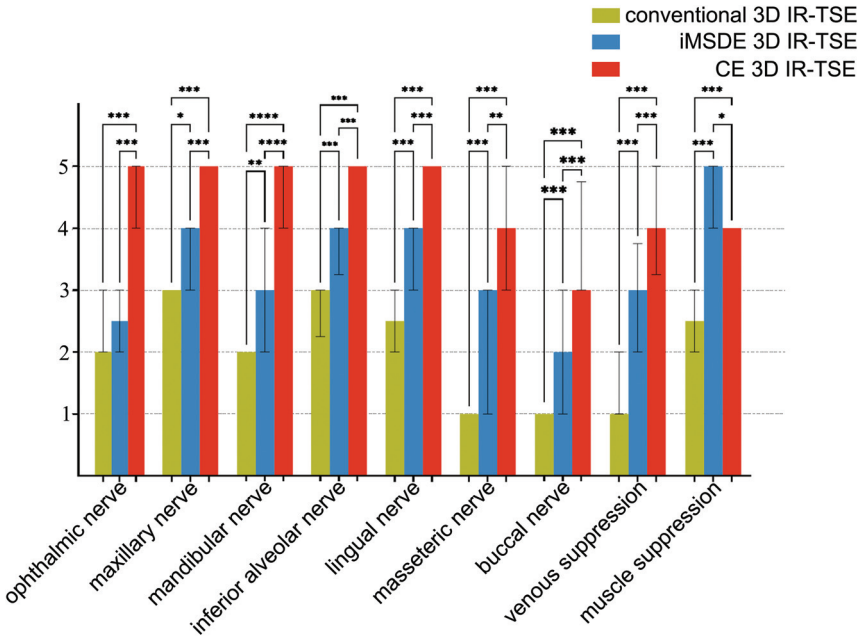

FIG 2. Comparisons of the visibility of 7 major peripheral branches of the trigeminal nerve and muscle/venous suppression among 3 sequences in 20 healthy subjects. The asterisk indicates $P <$ .05; double asterisks, $P <$ .01; triple asterisks, $P <$ .001; CE, contrast-enhanced.

3D IR-TSE showed the highest scores for venous suppression followed by iMSDE 3D IR-TSE (all $P <$ .05) (Figs 1 and 2).

For image diagnostic quality, as shown in the Online Supplemental Data, the number of MRN images with acceptable image quality (visualization scores ≥3) from iMSDE 3D IR-TSE was significantly higher than those from conventional 3D IR-TSE of the maxillary nerve, mandibular nerve, inferior alveolar nerve, lingual nerve, masseteric nerve, and buccal nerve (all $P <$ .05). Except for the buccal nerve and ophthalmic nerve, no significant difference in MRN images with acceptable image quality was found between the iMSDE 3D IR-TSE and the contrast-enhanced 3D IR-TSE in the maxillary nerve, mandibular nerve, inferior alveolar nerve, lingual nerve, and masseteric nerve (all $P >$ .05).

SNR, CR, and CNR Calculation of Normal Nerve

The SNR, CR, and CNR for nerves among the MRN sequences are summarized in the Online Supplemental Data. The SNR of the inferior alveolar nerve on iMSDE 3D IR-TSE was significantly lower than that on the conventional 3D IR-TSE ($P <$ .001) but was higher than that on the contrast-enhanced 3D IR-TSE ($P =$ .007) (Online Supplemental Data and Fig 3). The iMSDE 3D IR-TSE and contrast-enhanced 3D IR-TSE yielded significantly higher CR_{nv} and CNR_{nv} than conventional 3D IR-TSE (all $P <$ .001). However, the difference in CR_{nv} and CNR_{nv} between iMSDE 3D IR-TSE and contrast-enhanced 3D IR-TSE was not significant ($P =$ .615 for CR_{nv}, $P =$ .219 for CR_{nm}, respectively). Both CR_{nm} and CNR_{nm} on iMSDE 3D IR-TSE was significantly higher than on contrast-enhanced 3D IR-TSE ($P <$ .05).

There was moderate-to-excellent interobserver agreement regarding the SNR (ICC, 0.44–0.56), CR_{nv} (ICC, 0.84–0.92), CNR_{nv} (ICC, 0.55–0.88), CR_{nm} (ICC, 0.93–0.98), and CNR_{nm} (ICC, 0.45–0.57) (Online Supplemental Data).

Comparisons of Identification Ability of the Relationship between Nerves and Lesions

A total of 17 lesions in 15 patients were confirmed by pathology or clinical diagnosis, including 1 pituitary macroadenoma, 1 abscess, 4 nasopharyngeal carcinomas, 4 neurilemmomas, 1 hemangioma, 2 squamous carcinomas, and 1 meningioma (Online Supplemental Data). A total of 25 pairs of nerve-lesion relationships were evaluated. For identification ability, as shown in Figs 4 and 5, the iMSDE 3D IR-TSE (median [interquartile range] = 5 [1.5]) had highest scores compared with conventional 3D IR-TSE (median [interquartile range] = 3 [2]) and contrast-enhanced 3D IR-TSE (median [interquartile range] = 2 [4]) (all $P <$ .05).

DISCUSSION

The 3D IR-TSE sequence has been widely used in peripheral nerve MR imaging due to its high soft-tissue contrast and excellent fat suppression. However, there is still a challenge in imaging the extracranial branches of the trigeminal nerve due to the surrounding venous plexus and the requirement for contrast agents to homogeneously suppress venous signal.[23] Our results demonstrated that the iMSDE 3D IR-TSE sequence provides better

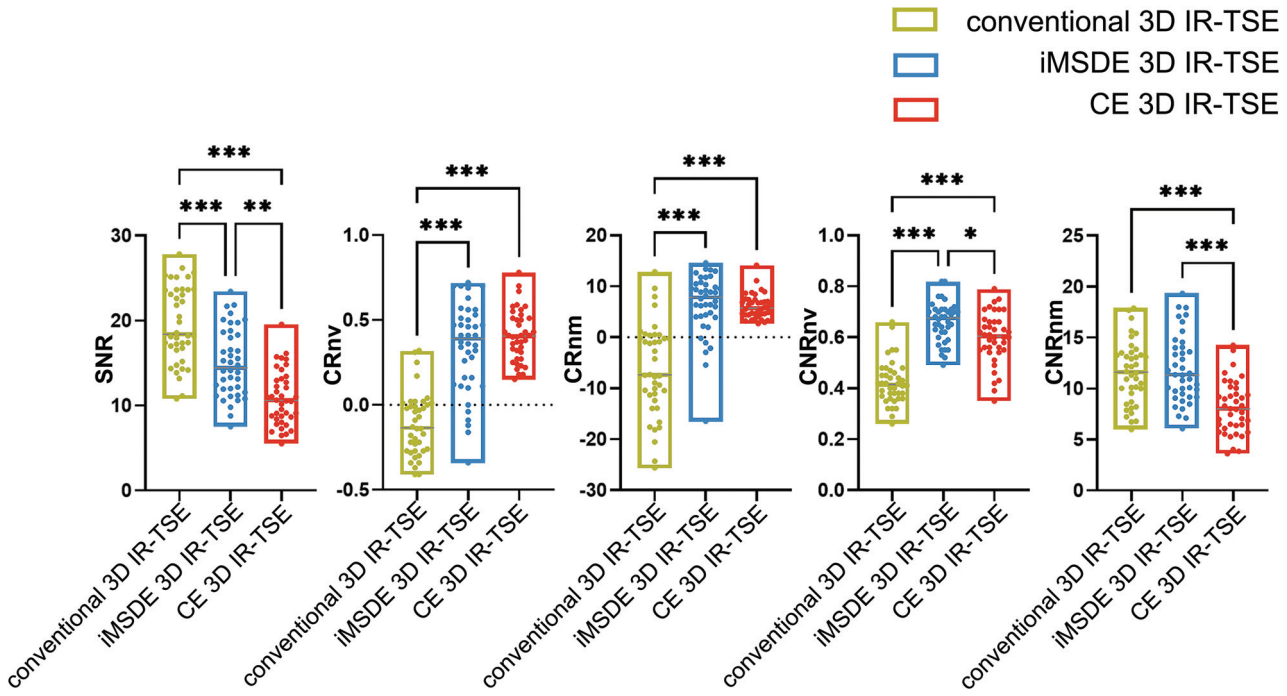

FIG 3. Comparisons of SNR, CR_{nv}, CNR_{nv}, CR_{nm}, and CNR_{nm} among 3 sequences in 20 subjects. The asterisk indicates $P < .05$; double asterisks, $P < .01$; triple asterisks, $P < .001$; CE, contrast-enhanced.

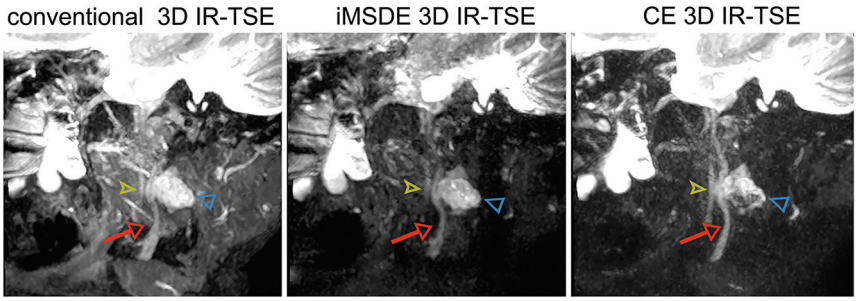

FIG 4. A 29-year-old patient with neurilemmoma. The sagittal image after MPR and MIP (3-mm layer thickness) shows that the neurilemmoma (*blue triangle*) compressed and moved the inferior alveolar nerve (*red thin arrow*) forward and the lingual nerve (*yellow arrowhead*) was not involved. Venous signals make nerves challenging to visualize on conventional 3D IR-TSE. CE indicates contrast-enhanced.

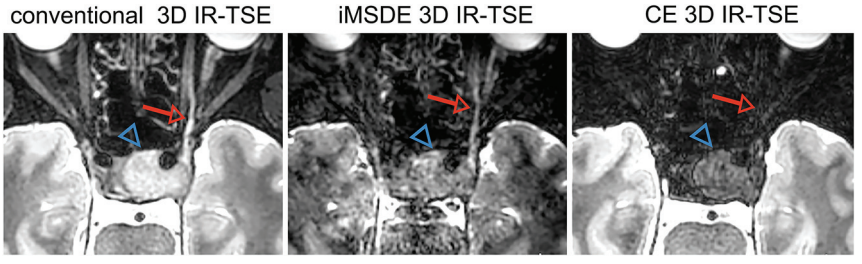

FIG 5. A 46-year-old patient with a large pituitary adenoma. The transverse image after MPR and MIP (3-mm layer thickness) demonstrates a large pituitary adenoma (*blue triangle*) invasion of the ophthalmic nerve (*red thin arrow*). The involved nerve and tumor are shown as low signal, which is difficult to identify on contrast-enhanced 3D IR-TSE. CE indicates contrast-enhanced.

venous suppression and nerve visualization than conventional 3D IR-TSE in imaging the extracranial branches of the trigeminal nerve. The visualization of the extracranial branches of the trigeminal nerve with iMSDE 3D IR-TSE is comparable with that of contrast-enhanced 3D IR-TSE.

The low contrast between nerve and adjacent tissue is a major problem affecting the imaging of the extracranial branches of the trigeminal nerve in the neck area, because these branches are surrounded by the hyperintense venous plexus along their course.[23] Gd-DTPA is routinely used for 3D IR-TSE in clinical practice to increase the contrast between nerve and background tissue. However, Gd-DTPA is not suitable for children and pregnant women. The signal of the background tissue was markedly decreased on the basis of the absorption of Gd-DTPA, while the signal of the nerve was not affected because the blood-nerve barrier hindered the nerve uptake of contrast agent.[15-17] Recently, 3D IR-TSE with iMSDE has been used to improve vessel signal suppression and visualization of nerves in the brachial plexus based on the additional motion-sensitizing gradient and T2 preparation pulse.[19,21,22] The present results showed that the venous suppression of both iMSDE 3D IR-TSE and contrast-enhanced 3D IR-TSE was improved compared to that of the conventional 3D IR-TSE. Compared with the contrast-enhanced 3D IR-TSE, the scores of venous

suppression were slightly lower in the iMSDE 3D IR-TSE. However, the quantitative CR_{nv} and CNR_{nv} were not significantly different between them. This finding suggested that the iMSDE preparation pulse effectively suppresses venous signals similar to the use of Gd-DTPA. In terms of muscle suppression, iMSDE 3D IR-TSE achieved the highest score among these 3 sequences, which was consistent with the quantitative results of the CR_{nm} and CNR_{nm}. This result indicated that iMSDE magnetization preparation was more effective in muscle suppression than the use of Gd-DTPA when applied to MR imaging of the trigeminal nerve.

Although the contrast-enhanced 3D IR-TSE allowed slightly better visualization of nerve than the iMSDE 3D IR-TSE, the diagnostic quality of the image in most trigeminal nerve branches was comparable between these 2 sequences. It suggested that the additional iMSDE pulse brought uniform venous and muscle suppression and improved visualization of most branches of the trigeminal nerve. However, there was still a challenge in visualizing the ophthalmic nerve by iMSDE 3D IR-TSE, despite the enhanced background tissue suppression. This challenge can be explained by the motion-sensitive nature of the iMSDE preparation pulse, leading to unsatisfactory visualization of ophthalmic nerve caused by eye movement. In addition, the visualization score of the buccal nerve was relatively low in all 3 sequences, resulting from the small nerve diameter and proximity to the pterygoid plexus.

As for the evaluation of the relationship between nerves and lesions, studies have shown that the CISS sequence, which is a type of negative contrast neurography technique, was feasible in determining the location of the facial nerve relative to tumor.[26] In addition, it has been widely reported that contrast-enhanced 3D IR-TSE had an excellent performance in assessing the extracranial trigeminal nerve branches, which can potentially have head and neck tumors. However, fewer studies have investigated the value of contrast-enhanced 3D IR-TSE to identify the relationship between nerves and lesions. Most interesting, our results showed that Gd-DTPA could decrease the signal of lesions and damaged nerves, leading to poor determination of the relationship between nerves and lesions. Therefore, it was difficult to identify the spatial relationship between nerves and lesions using contrast-enhanced 3D IR-TSE. On the contrary, the analyses showed that iMSDE 3D IR-TSE provided significantly higher scores in identifying nerve-lesion relationships compared with contrast-enhanced 3D IR-TSE. This finding is probably because the iMSDE preparation pulse did not decrease the signal of the lesions, yielding relatively high contrast between nerves and lesions.

There were still several limitations to our study. First, this prospective study recruited only a relatively small number of patients, and some of them were only clinically diagnosed but not pathologically confirmed. Therefore, more patients are required to further verify the benefits of these sequences in evaluating different pathologic conditions involving the trigeminal nerve. Second, the performance of identifying the relationship between nerves and lesions was not compared between iMSDE 3D IR-TSE and a conventional contrast-enhanced T1-weighted sequence. Third, the analytic approach did not account for within-patient correlation due to the inclusion of multiple nerves per patient. Finally, the acquisition time of 3D IR-TSE in our study was still relatively long; thus, new technologies such as compressed sensing are needed in our future investigations.[27]

CONCLUSIONS

iMSDE 3D IR-TSE outperformed conventional 3D IR-TSE in providing better venous/muscle suppression and image quality. Furthermore, compared with contrast-enhanced 3D IR-TSE, iMSDE 3D IR-TSE offers a comparable visualization of most extracranial trigeminal nerve branches and better identifies the relationship between nerves and lesions. Therefore, iMSDE 3D IR-TSE is a promising alternative to contrast-enhanced 3D IR-TSE in visualizing the extracranial branches of the trigeminal nerve in clinical practice.

Disclosure forms provided by the authors are available with the full text and PDF of this article at www.ajnr.org.

REFERENCES

1. Bathla G, Hegde AN. **The trigeminal nerve: an illustrated review of its imaging anatomy and pathology.** *Clin Radiol* 2013;68:203–13 CrossRef Medline
2. Borges A, Casselman J. **Imaging the cranial nerves, Part I: methodology, infectious and inflammatory, traumatic and congenital lesions.** *Eur Radiol* 2007;17:2112–25 CrossRef Medline
3. Borges A, Casselman J. **Imaging the cranial nerves, Part II: primary and secondary neoplastic conditions and neurovascular conflicts.** *Eur Radiol* 2007;17:2332–44 CrossRef Medline
4. Chhabra A, Bajaj G, Wadhwa V, et al. **MR neurographic evaluation of facial and neck pain: normal and abnormal craniospinal nerves below the skull base.** *Radiographics* 2018;38:1498–513 CrossRef Medline
5. Hyare H, Wisco JJ, Alusi G, et al. **The anatomy of nasopharyngeal carcinoma spread through the pharyngobasilar fascia to the trigeminal mandibular nerve on 1.5 T MRI.** *Surg Radiol Anat* 2010; 32:937–44 CrossRef Medline
6. Cox B, Zuniga JR, Panchal N, et al. **Magnetic resonance neurography in the management of peripheral trigeminal neuropathy: experience in a tertiary care centre.** *Eur Radiol* 2016;26:3392–400 CrossRef Medline
7. Dercle L, Hartl D, Rozenblum-Beddok L, et al. **Diagnostic and prognostic value of 18F-FDG PET, CT, and MRI in perineural spread of head and neck malignancies.** *Eur Radiol* 2018;28:1761–70 CrossRef Medline
8. Dessouky R, Xi Y, Zuniga J, et al. **Role of MR neurography for the diagnosis of peripheral trigeminal nerve injuries in patients with prior molar tooth extraction.** *AJNR Am J Neuroradiol* 2018;39:162–69 CrossRef Medline
9. Blitz AM, Choudhri AF, Chonka ZD, et al. **Anatomic considerations, nomenclature, and advanced cross-sectional imaging techniques for visualization of the cranial nerve segments by MR imaging.** *Neuroimaging Clin N Am* 2014;24:1–15 CrossRef Medline
10. Fujii H, Fujita A, Yang A, et al. **Visualization of the peripheral branches of the mandibular division of the trigeminal nerve on 3D double-echo steady-state with water excitation sequence.** *AJNR Am J Neuroradiol* 2015;36:1333–37 CrossRef Medline
11. Kikuchi T, Fujii H, Fujita A, et al. **Visualization of the greater and lesser occipital nerves on three-dimensional double-echo steady-state with water excitation sequence.** *Jpn J Radiol* 2020;38:753–60 CrossRef Medline
12. Zhang Z, Meng Q, Chen Y, et al. **3-T imaging of the cranial nerves using three-dimensional reversed FISP with diffusion-weighted MR sequence.** *J Magn Reson Imaging* 2008;27:454–58 CrossRef Medline
13. Chu J, Zhou Z, Hong G, et al. **High-resolution MRI of the intraparotid facial nerve based on a microsurface coil and a 3D reversed fast imaging with steady-state precession DWI sequence at 3T.** *AJNR Am J Neuroradiol* 2013;34:1643–48 CrossRef Medline

14. Viallon M, Vargas MI, Jlassi H, et al. **High-resolution and functional magnetic resonance imaging of the brachial plexus using an isotropic 3D T2 STIR (Short Term Inversion Recovery) SPACE sequence and diffusion tensor imaging.** *Eur Radiol* 2008;18:1018–23 CrossRef Medline
15. Wu W, Wu F, Liu D, et al. **Visualization of the morphology and pathology of the peripheral branches of the cranial nerves using three-dimensional high-resolution high-contrast magnetic resonance neurography.** *Eur J Radiol* 2020;132:109137 CrossRef Medline
16. Wang L, Niu Y, Kong X, et al. **The application of paramagnetic contrast-based T2 effect to 3D heavily T2W high-resolution MR imaging of the brachial plexus and its branches.** *Eur J Radiol* 2016; 85:578–84 CrossRef Medline
17. Zhang Y, Kong X, Zhao Q, et al. **Enhanced MR neurography of the lumbosacral plexus with robust vascular suppression and improved delineation of its small branches.** *Eur J Radiol* 2020;129:109128 CrossRef Medline
18. Fraum TJ, Ludwig DR, Bashir MR, et al. **Gadolinium-based contrast agents: a comprehensive risk assessment.** *J Magn Reson Imaging* 2017;46:338–53 CrossRef Medline
19. Yoneyama M, Takahara T, Kwee TC, et al. **Rapid high-resolution MR neurography with a diffusion-weighted pre-pulse.** *Magn Reson Med Sci* 2013;12:111–19 CrossRef Medline
20. Srinivasan S, Hu P, Kissinger KV, et al. **Free-breathing 3D whole-heart black-blood imaging with motion sensitized driven equilibrium.** *J Magn Reson Imaging* 2012;36:379–86 CrossRef Medline
21. Kasper JM, Wadhwa V, Scott KM, et al. **SHINKEI–a novel 3D isotropic MR neurography technique: technical advantages over 3DIRTSE-based imaging**. *Eur Radiol* 2015;25:1672–77 CrossRef Medline
22. Klupp E, Cervantes B, Sollmann N, et al. **Improved brachial plexus visualization using an adiabatic iMSDE-prepared STIR 3D TSE.** *Clin Neuroradiol* 2019;29:631–38 CrossRef Medline
23. Van der Cruyssen F, Croonenborghs TM, Hermans R, et al. **3D cranial nerve imaging, a novel MR neurography technique using black-blood STIR TSE with a pseudo steady-state sweep and motion-sensitized driven equilibrium pulse for the visualization of the extraforaminal cranial nerve branches.** *AJNR Am J Neuroradiol* 2021;42:578–80 CrossRef Medline
24. Deshmukh S, Tegtmeyer K, Kovour M, et al. **Diagnostic contribution of contrast-enhanced 3D MR imaging of peripheral nerve pathology.** *Skeletal Radiol* 2021;50:2509–18 CrossRef Medline
25. Benjamini Y, Krieger AM, Yekutieli D. **Adaptive linear step-up procedures that control the false discovery rate.** *Biometrika* 2006; 93:491–507 CrossRef
26. Guenette JP, Ben-Shlomo N, Jayender J, et al. **MR imaging of the extracranial facial nerve with the CISS sequence.** *AJNR Am J Neuroradiol* 2019;40:1954–59 CrossRef Medline
27. Aoike T, Fujima N, Yoneyama M, et al. **Development of three-dimensional MR neurography using an optimized combination of compressed sensing and parallel imaging.** *Magn Reson Imaging* 2022;87:32–37 CrossRef Medline